Superconducting DC busbar with low resistive joints for all-electric aircraft propulsion system

Gaurav Gautam[a], Min Zhang[a], Weijia Yuan[a], Graeme Burt[a] and Daniel Malkin[b]

[a]University of Strathclyde, 16 Richmond St, Glasgow, G1 1XQ, United Kingdom
[b]GKN Aerospace, Taurus Rd, Patchway, Filton, BS34 6FB, Bristol, United Kingdom

ARTICLE INFO

Keywords:
Superconducting busbar
Carbon emission
All-electric aircraft
High current
Joints
Critical current
Power cycling
Thermal cycling

ABSTRACT

High-temperature superconductors (HTS) can carry high currents with almost zero loss when transmitting direct current (DC). Their compact size and lower weight make them suitable for the application of all-electric aircraft. However, the current carrying capability of a single HTS tape is limited to a few hundred amps; therefore, for high-current applications, multiple HTS tapes need to be connected in parallel. The flat geometry of HTS tape and its critical current (IC) dependence on strain complicate grouping them in parallel. Furthermore, the length of HTS tape is limited by its crystal structure, necessitating low-resistance joints for extended applications. A superconducting busbar design for high-current applications is developed and tested to address these challenges. The superconducting busbar is designed in a way that it helps to reduce the effect of the self-field on critical current and also ride through the fault events. Yttrium barium copper oxide (YBCO) tapes are used to develop the busbar prototype, tested against DC currents in a liquid nitrogen environment. Joint optimization is carried out to determine the required length for efficiently joining HTS tapes. Two busbar prototypes are developed with 180° and 90° joints to join 5 HTS tapes and tested in self-field. A joint resistance of 100 $n\Omega$ is measured at self-field for the 180° joint busbar, and 800 $n\Omega$ is measured for the 90° joint busbar. Both busbar prototypes are subjected to power cycling and thermal cycling to assess joint performance in self-field and any degradation of the joint electrical parameters during testing.

1. Introduction

Aviation emissions are one of the major contributors to global warming and climate change. Flightpath 2050, is an ambitious goal for the aviation sector, setting targets to reduce Carbon Dioxide (CO_2) by 75%, Oxides of Nitrogen (NOx) by 90% and noise emissions by 65% compared to aircraft of the year 2000 [6]. Advancements in engine technologies can contribute to reaching these goals to a certain degree, but to fully realize this target the development of new technologies is essential. Aircraft electrification is seen as a key solution to meet these targets. The More Electric Aircraft's (MEA) concept demonstrated that replacing traditional sub-systems with electric systems reduces weight, fuel consumption, and noise emission, Boieng 787, and Airbus A380 are examples of MEA [17]. All-electric aircraft are required to achieve the 2050 target, which requires a significant increase in onboard power requirements [4]. Early research indicates that the distributed propulsion system concept is a prominent architecture for all-electric aircraft [11]. NASA's N3-X wide-body aircraft is such a concept designed for 300 passengers and requires 22.4 MVA of power from each turbo-shaft engine [2].

Conventional copper and aluminum-based power distribution systems are not suitable for all-electric aircraft due to their weight, size, and power loss. A study in [1], suggests superconducting systems for all-electric aircraft due to their power-to-weight ratio. A DC power system is prominent due to its low losses and the ability to decouple power and thrust generation through converters. An example of a basic architecture for electric aircraft is shown in Fig. 1 [14]. The architecture has three main components: power source, electric power distribution system, and distributed propulsion unit. A superconducting busbar is a part of the power distribution system that carries a high current and connects the source with the load. A superconducting busbar requires multiple HTS tapes connected in parallel, for grouping HTS tapes there are three different approaches: the Robel concept [9, 3], the co-axial winding concept [19, 5, 10, 18], and the stack concept [16, 15]. The stack concept is used in this work to develop superconducting busbar prototypes.

In this work, we have developed a design for a superconducting busbar for high-current applications, equipped with low-resistance 180° and 90° joints. The joint area is carefully optimized to ensure minimal resistance, enhancing the system's overall efficiency. The busbar design is distinct as it is also equipped with a design that helps to reduce the effect of self-field on critical current and withstand fault events. A prototype of the superconducting busbar was prepared and tested in the lab environment. The busbar was subjected to power and thermal cycling to assess its reliability and durability.

This paper is structured as follows: Section 2 explains the role of superconductivity in all-electric aircraft. Section 3 outlines the mechanical structure and the methodology for joint implementation. Section 4 covers the experimental setup and presents the experimental results, which include an analysis of joint resistance and power loss during testing,

gaurav.gautam@strath.ac.uk (G. Gautam); min.zhang@strath.ac.uk (M. Zhang); min.zhang@strath.ac.uk (W. Yuan); graeme.burt@strath.ac.uk (G. Burt); daniel.malkin@gknaerospace.com (D. Malkin)
ORCID(s): 0000-0002-0754-7506 (G. Gautam)

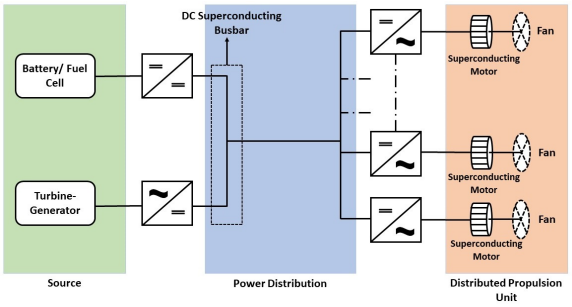

Figure 1: Basic architecture of electric aircraft.

and a discussion of the impact of power and thermal cycling on the joint performance. Section IV presents the conclusions drawn from this research.

2. Role of superconductivity in all-electric aircraft

For all-electric aircraft, the power requirements are significantly higher than for conventional aircraft, reaching the megawatt (MW) range. The increased onboard power requirement for different classes of electric aircraft is predicted in [4]. As power demand increases, voltage levels are raised to reduce conductor weight. While increasing voltage helps lower the current, thereby decreasing resistive losses, it also necessitates thicker insulation, which adds to conductor weight. Conventional conductors are unsuitable for these applications due to their low power-to-weight ratio. In contrast, superconductors offer a high power-to-weight ratio with minimal heat losses. Traditional aircraft use a DC power system following the MIL-STD-704 standard, a two-wire configuration supporting either 28 V or 270 V [12]. This voltage standard is widely used in aviation and is based on Paschen's law, which dictates that at standard conditions, a minimum of 327 V DC is required to trigger a voltage breakdown. To prevent electrical breakdown, aircraft power systems are typically designed to operate below this 327 V DC threshold. However, in all-electric aircraft, the power system will operate at much lower temperatures, where voltage breakdown characteristics change as a function of temperature. At these reduced temperatures, the breakdown voltage increases, potentially allowing the system to operate safely at higher voltages. The CHEETA project proposes a drivetrain with a voltage of 1 kV and a current range of 0-20 kA [13]. This shift presents an opportunity to design higher-voltage systems with superconductors, which can support increased power transmission with minimal weight and heat loss.

3. Mechanical Structure and Joints of Busbar

The stack concept is used to develop superconducting busbar prototypes [7]. Two prototypes of superconducting busbars are developed, each incorporating a distinct design: one with a 180° lap-to-lap joint and the other with a 90° lap-to-lap joint. Both prototypes utilized second-generation

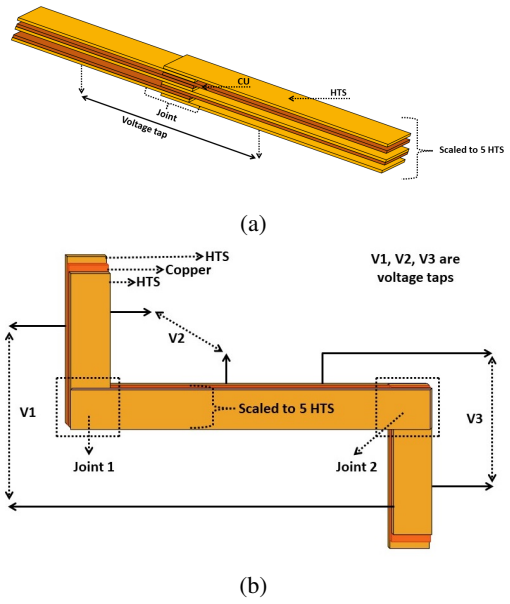

Figure 2: (a) Superconducting busbar with 180° lap-to-lap joint scaled to 4 copper tapes sandwiched between 5 HTS tapes. (b) Superconducting busbar with 90° lap-to-lap joint scaled to 4 copper tapes sandwiched between 5 HTS tapes.

(2G), 4-mm wide YBCO tapes produced by Shanghai Superconductors with a critical current (IC) of 120 A and 4 mm wide copper tape, as shown in Fig. 2. Copper is added in between HTS tapes acts like a stabilizer and help to ride through fault events. Copper between HTS tapes also adds a gap between HTS tapes and helps to reduce the effect of self-field on critical current. Copper carries current only during transients or fault states and doesn't carry current during steady state, explained briefly by authors in [8]. This work is an extension of the previous work by the authors [8], where mechanical structure in terms of laying HTS and copper tapes is explained. This work focuses on the development of a busbar design with low-resistive joints which is used to connect multiple HTS tapes.

3.1. Busbar with 180° joint

The length of HTS tape is limited, for extended applications joining HTS tapes is necessary, as illustrated in Fig. 2a. For a low-resistance joint, the superconducting side of the HTS tape is used to join other HTS tapes. Due to the HTS layered structure, the substrate side of the HTS tape should be avoided when making a joint to reduce joint resistance. In the process of joint development, the first step is to treat the HTS and copper tapes with flux, which removes oxides from the surface of the tapes and helps to spread the soldering material evenly across the HTS tape surface. Four copper tapes are sandwiched between five HTS tapes and joined together, as shown in Fig. 2a. Lead-tin (PbSn) based solder is applied throughout the entire surface of the tapes and heated to 200°C for 20-25 minutes while applying mechanical pressure through the former. The temperature and duration of the process vary based on several factors

like the melting temperature of the solder, the material of the former, and the thickness of the former.

3.1.1. Optimization of 180° joint length:

The length of a 180° lap-to-lap joint is optimized to 3cm - 4 cm, with a joint area of 1.2 cm^2 to 1.6 cm^2 based on multiple experiments. The experiments ranged from 1 cm to 4 cm joint length, comparing their Voltage-Current (VI) characteristics with HTS tape having no joint. As shown in Fig. 3, the optimal joint length for a 4 mm HTS tape is 3cm to 4 cm. This length achieves almost the same IC as an HTS tape without a joint, according to $1\mu V$ criteria. Additionally, the 3 cm to 4 cm joint demonstrates less resistance and power loss, 100 $n\Omega$ and 0.001 W during the DC test, compared to the 1 cm to 2 cm joint length shown in Fig. 4. This indicates that resistance of the joint depends upon the area of the joint. Further, in this work based on experiments, 3 cm to 4 cm lap-to-lap joints are used for busbar prototypes.

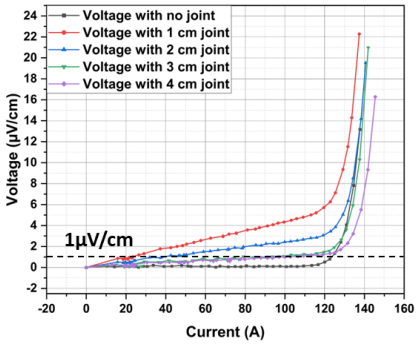

Figure 3: V-I characteristics for varying joint lengths to determine the optimal joint length.

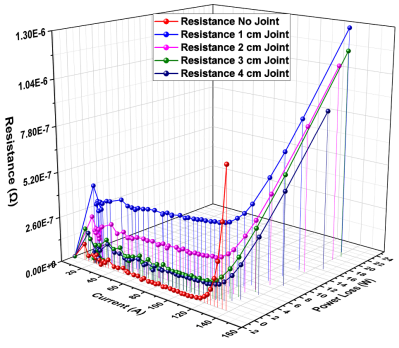

Figure 4: Joint resistance and power loss w.r.t to current for different joint lengths.

3.2. Busbar with 90° joint

The design of the 90° joint is more complex compared to the 180° joint due to spatial arrangement. Unlike the 180° joint, the 90° joint doesn't have room to change the area of the joint, making it more resistive compared to the 180° joint. In the 90° joint, the area of the joint can only be increased by changing the HTS tape width from 4 mm to 6 mm or 12 mm. One complexity of this joint design is that, due to the additional copper placed between HTS tapes at the joint where the HTS tapes intersect during manufacturing, the superconducting material may break under mechanical pressure. This occurs because the copper tape is added between the HTS tapes. To address this challenge, the copper tapes are precisely cut and transposed between the HTS tapes to avoid breakage. A busbar prototype is developed with 4 copper tapes sandwiched between 5 HTS tapes, resulting in a joint area of 0.16 cm^2 as shown in Fig. 5b. Two 90° joints are implemented while joining 5 HTS tapes, as shown in Fig. 2b. The same procedure used to design the 180° joint is employed for 90° joint implementation.

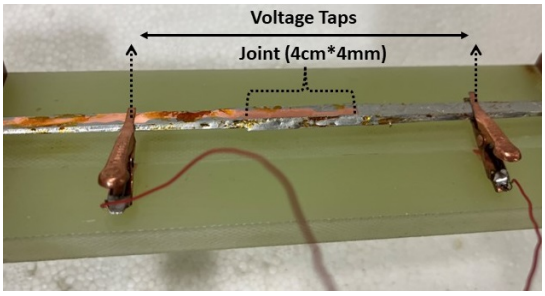

(a)

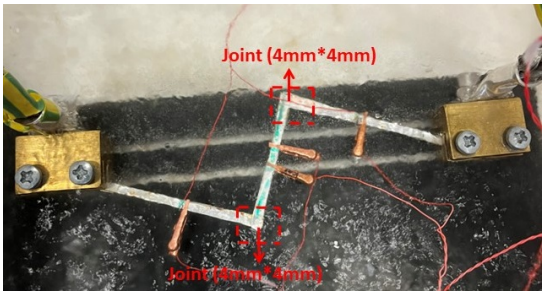

(b)

Figure 5: (a) 5 HTS tapes and 4 copper tapes busbar with 180° lap-to-lap joint. (b) 5 HTS tapes and 4 copper tapes busbar with two 90° lap-to-lap joint.

4. Experimental Setup and Results

The experiments are conducted using a TDK-GSP10-1000-3P400 programmable DC power supply, capable of delivering up to 10 kW of power, with a maximum output current of 1 kA and an output voltage range of 0 - 10 V. The power supply features a USB interface, allowing communication with the host computer. This communication enables precise control of the power supply during the experiments. Experiments are conducted with the liquid nitrogen (LN2) environment in an open bath cryostat. Current is pushed through the HTS busbar with the help of copper terminals, which are also immersed in the LN2 to minimize heat leakage. The Shunt measures the current passing through the HTS busbar, and voltage taps measure the voltage across the joint. A program is developed in LabVIEW to control

Table 1
Measured electrical resistance of the superconducting busbar with 180° and 90° joints during test

Parameter	Busbar with 180 Joint	Busbar with 90° Joint
Total Applied Current	600 A	600 A
Number of HTS	5	5
Number of copper tapes	4	4
Width of HTS tapes	4 mm	4 mm
Width of copper tapes	4 mm	4 mm
Resistance	100 $n\Omega$	1.6 $\mu\Omega$
Power Loss	0.03 W	0.4 W
Resistance (Joint 1)	-	800 $n\Omega$
Power Loss (Joint 1)	-	0.2 W
Resistance (Joint 2)	-	800 $n\Omega$
Power Loss (Joint 2)	-	0.2 W

the operation and data acquisition, for which a National Instruments NI-9238 voltage input module, with a cDAQ-9174 chassis, is used. The layout of the experimental setup is shown in Fig. 6.

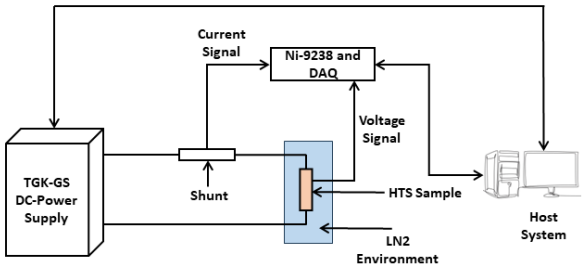

Figure 6: Schematic of the experimental setup used to perform experiments.

4.1. Busbar test with 180° joint

A Superconducting busbar prototype with 180° joint which joins 5 HTS tapes, with 4 copper tapes in between HTS tapes is developed, as illustrated in Fig. 2a. 600 A DC is pushed through the busbar with DC power supply and V-I characteristics is measured. Table 1 outlines the electrical parameters obtained during the test. Superconducting busbar with 180° joint demonstrates 100 $n\Omega$ joint resistance and power losses is less than 0.05 W as shown in Fig. 8, V-I curve is shown in Fig. 7. To ensure the reliability and durability of the busbar joint, the busbar is subjected to power cycling and thermal cycling. Power cycling is done by repeating the power test, and thermal cycling involves subjecting a superconducting busbar prototype to temperature fluctuations by transferring it between room temperature and liquid nitrogen temperature. Both these processes are repeated 11 times and results are compared to observe any degradation in electrical parameters of the superconducting busbar. V-I curve is compared in Fig. 9, resistance and power loss w.r.t current is compared in Fig. 10, show no degradation in electrical parameters during the test.

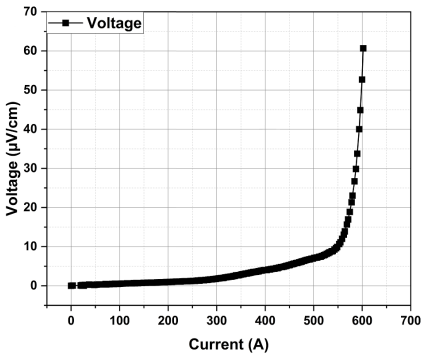

Figure 7: V-I characteristic of a 180° lap-to-lap joint incorporating 5 HTS tapes and 4 copper tapes.

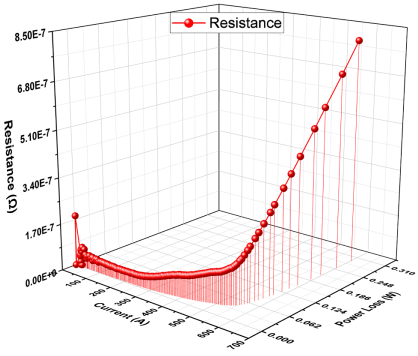

Figure 8: Joint resistance and power loss of 180° lap-to-lap joint w.r.t to current.

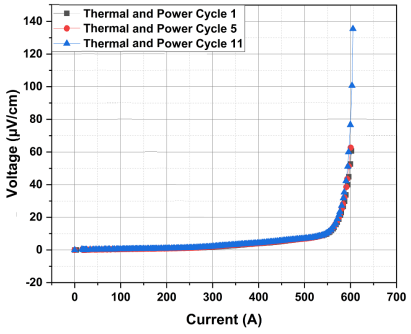

Figure 9: V-I characteristic of a 180° lap-to-lap joint with 5 HTS tapes and 4 copper tapes undergoing power and thermal cycling.

4.2. Busbar test with 90° joint

A superconducting busbar is developed with two 90° joints while connecting multiple HTS tapes, which join 5 HTS tapes and 4 copper tapes sandwiched between HTS tapes, as shown in Fig. 2b. The busbar prototype is tested with the help of a DC power supply, which is used to push 600 A through the busbar, and V-I characteristics are

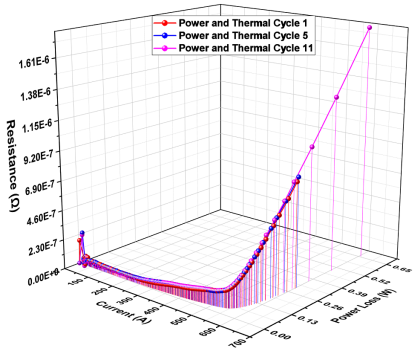

Figure 10: Joint resistance and power loss of 180° joint w.r.t to current, during 11 times power and thermal cycling.

measured. Voltage is measured across each joint (i.e. joint 1 and joint 2) to measure power loss and resistance across each joint, and across both joints, as shown in Fig. 2b, to measure overall resistance and power loss across both joints. Busbar demonstrates resistance across both joints is 1.6 $\mu\Omega$ with a power loss of 0.4 W, as shown in Fig. 12. Resistance across each joint (joint 1 and joint 2) is 800 $n\Omega$, and power loss across each joint is 0.2 W, as shown in Fig. 12. V-I characteristic of the superconducting busbar obtained during the test is shown in Fig. 11. Power cycling and thermal cycling are implemented to see any degradation in the electrical parameters of the superconducting busbar joint. Power and thermal cycling is repeated 11 times and results are compared, V-I curve is shown in Fig. 13, and power loss and resistance w.r.t current is shown in Fig. 14. Repeated graphs show reliability and multiple tests show the durability of the joints.

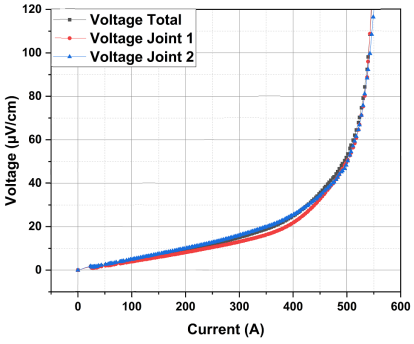

Figure 11: V-I characteristic of two 90° lap-to-lap joints incorporating 5 HTS tapes and 4 copper tapes.

5. Conclusion

A superconducting busbar prototype is developed and tested against high currents for high-power applications. Single HTS tape current carrying capability is limited to a few hundred amps, for high-current applications there is a need to connect multiple HTS tapes in parallel. Joining multiple HTS tapes with low-resistance joints is one of the challenge addressed in this work, while make sure that the

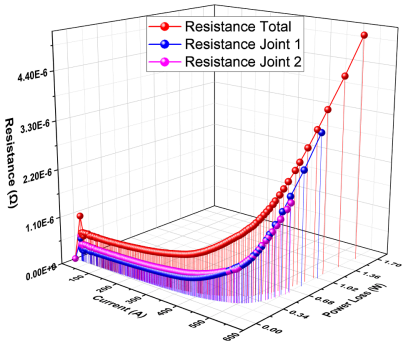

Figure 12: Joint resistance and power loss w.r.t to the current of two 90° joints.

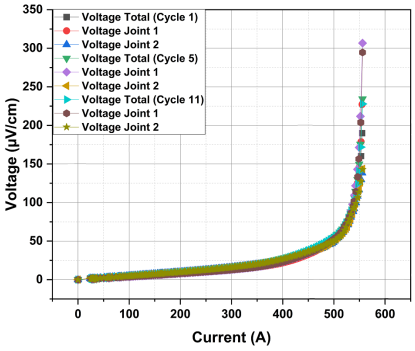

Figure 13: V-I characteristic of two 90° lap-to-lap joints with 5 HTS tapes and 4 copper tapes subjected to 11 times power and thermal cycles.

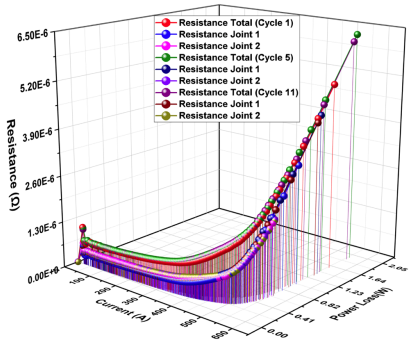

Figure 14: Joint resistance and power loss of 90° joint w.r.t to current during power and thermal cycling.

busbar design allows reduced effect of self field on critical current and ride through fault events. 180° and 90° joints are implemented to join multiple HTS tapes and tested. A total joint resistance of 100 $n\Omega$ and a power loss of 0.03 W is obtained while connecting 5 HTS tapes with lap-to-lap 180° joint. Two 90° joints exhibit a total resistance of 1.6 $\mu\Omega$ and a power loss of 0.4 W while connecting 5 HTS tapes with 4 copper tapes sandwiched between the HTS tapes. Each 90° joint has a resistance of 800 $n\Omega$ and a power loss of 0.2 W. The joint resistance depends upon the joint area, therefore, the 90° joint possesses more resistance than

the 180° joint. To ensure the durability and reliability of the busbar joints, the busbar is subjected to power cycling and thermal cycling. Both tests are conducted 11 times, and the results are compared to check the performance of the superconducting busbar and to observe any potential degradation in electrical parameters. Results show that minimal degradation in electrical parameters is observed during testing, which shows that the design of busbar is reliable and durable for high-current applications.

Acknowledgement

This work was funded by the University of Strathclyde, Glasgow, United Kingdom, and GKN Aerospace Taurus Rd, Patchway, Filton, Bristol, United Kingdom.

References

[1] Armstrong, M., Blackwelder, M.J., Bollman, A.M., Ross, C.A.H., Campbell, A., Jones, C.E., Norman, P.J., 2015. Architecture, voltage and components for a turboelectric distributed propulsion electric grid. URL: https://api.semanticscholar.org/CorpusID:108680172.

[2] Armstrong, M., Ross, C.A.H., Phillips, D., Blackwelder, M.J., 2013. Stability, transient response, control, and safety of a high-power electric grid for turboelectric propulsion of aircraft. URL: https://api.semanticscholar.org/CorpusID:108189179.

[3] Bayer, C.M., Gade, P.V., Barth, C., Preuß, A., Jung, A., Weiß, K.P., 2015. Mechanical reinforcement for racc cables in high magnetic background fields. Superconductor Science and Technology 29, 025007. URL: https://dx.doi.org/10.1088/0953-2048/29/2/025007, doi:10.1088/0953-2048/29/2/025007.

[4] Buticchi, G., Wheeler, P., Boroyevich, D., 2023. The more-electric aircraft and beyond. Proceedings of the IEEE 111, 356–370. doi:10.1109/JPROC.2022.3152995.

[5] Choi, Y.S., Kim, D.L., Yang, H.S., Sohn, S.H., Lim, J.H., Hwang, S.D., 2011. Progress on the performance test of kepco hts power cable. IEEE Transactions on Applied Superconductivity 21, 1034–1037. doi:10.1109/TASC.2010.2093496.

[6] Commission, E., for Mobility, D.G., Transport, for Research, D.G., Innovation, 2011. Flightpath 2050 – Europe's vision for aviation – Maintaining global leadership and serving society's needs. Publications Office. doi:doi/10.2777/50266.

[7] Elschner, S., Brand, J., Goldacker, W., Hollik, M., Kudymow, A., Strauss, S., Zermeno, V., Hanebeck, C., Huwer, S., Reiser, W., Noe, M., 2018. 3s–superconducting dc-busbar for high current applications. IEEE Transactions on Applied Superconductivity 28, 1–5. doi:10.1109/TASC.2018.2797521.

[8] Gautam, G., Zhang, M., Yuan, W., Burt, G., Malkin, D., 2024. Fault tolerant superconducting busbar with reduced self-field effect on critical current design for all electric aircraft. IEEE Transactions on Applied Superconductivity 34, 1–5. doi:10.1109/TASC.2024.3351610.

[9] Goldacker, W., Grilli, F., Pardo, E., Kario, A., Schlachter, S.I., Vojenčiak, M., 2014. Roebel cables from rebco coated conductors: a one-century-old concept for the superconductivity of the future. Superconductor Science and Technology 27, 093001. URL: https://dx.doi.org/10.1088/0953-2048/27/9/093001, doi:10.1088/0953-2048/27/9/093001.

[10] Lee, S., Yoon, J., Lee, B., Yang, B., 2011. Modeling of a 22.9kv 50mva superconducting power cable based on pscad/emtdc for application to the icheon substation in korea. Physica C: Superconductivity and its Applications 471, 1283–1289. URL: https://www.sciencedirect.com/science/article/pii/S0921453411002668, doi:https://doi.org/10.1016/j.physc.2011.05.179. the 23rd International Symposium on Superconductivity.

[11] Loder, D.C., Bollman, A., Armstrong, M.J., 2018. Turbo-electric distributed aircraft propulsion: Microgrid architecture and evaluation for eco-150, in: 2018 IEEE Transportation Electrification Conference and Expo (ITEC), pp. 550–557. doi:10.1109/ITEC.2018.8450180.

[12] Madonna, V., Giangrande, P., Galea, M., 2018. Electrical power generation in aircraft: Review, challenges, and opportunities. IEEE Transactions on Transportation Electrification 4, 646–659. doi:10.1109/TTE.2018.2834142.

[13] Sebastian, M.A.P., Haugan, T.J., Kovacs, C.J., 2021. Design and scaling laws of a 40-mw-class electric power distribution system for liquid-h2 fuel-cell propulsion, in: 2021 AIAA/IEEE Electric Aircraft Technologies Symposium (EATS), pp. 1–12. doi:10.23919/EATS52162.2021.9704850.

[14] Terao, Y., Ishida, Y., Ohsaki, H., 2021. High-output density partial superconducting motors for aviation systems. Journal of Physics: Conference Series 1857, 012017. URL: https://dx.doi.org/10.1088/1742-6596/1857/1/012017, doi:10.1088/1742-6596/1857/1/012017.

[15] Terazaki, Y., Yanagi, N., Ito, S., Kawai, K., Seino, Y., Ohinata, T., Tanno, Y., Natsume, K., Hamaguchi, S., Noguchi, H., Tamura, H., Mito, T., Hashizume, H., Sagara, A., 2014. Critical current measurement of 30 ka-class hts conductor samples. IEEE Transactions on Applied Superconductivity 24, 1–5. doi:10.1109/TASC.2013.2287715.

[16] Terazaki, Y., Yanagi, N., Ito, S., Seino, Y., Hamaguchi, S., Tamura, H., Mito, T., Hashizume, H., Sagara, A., 2015. Measurement and analysis of critical current of 100-ka class simply-stacked hts conductors. IEEE Transactions on Applied Superconductivity 25, 1–5. doi:10.1109/TASC.2014.2377793.

[17] Wheeler, P., Bozhko, S., 2014. The more electric aircraft: Technology and challenges. IEEE Electrification Magazine 2, 6–12.

[18] Yang, B., Kang, J., Lee, S., Choi, C., Moon, Y., 2015. Qualification test of a 80 kv 500 mw hts dc cable for applying into real grid. IEEE Transactions on Applied Superconductivity 25, 1–5. doi:10.1109/TASC.2015.2396683.

[19] Yumura, H., Ashibe, Y., Itoh, H., Ohya, M., Watanabe, M., Masuda, T., Weber, C.S., 2009. Phase ii of the albany hts cable project. IEEE Transactions on Applied Superconductivity 19, 1698–1701. doi:10.1109/TASC.2009.2017865.